Low Energy Mesons in the Atmosphere*

MATTHEW SANDS
Department of Physics and Laboratory for Nuclear Science and Engineering, Massachusetts Institute of Technology, Cambridge, Massachusetts
(Received October 5, 1949)

The dependence on altitude of the intensity of slow mesons, mesons with ranges less than 100 g cm^{-2}, has been measured by the method of delayed coincidences for atmospheric depths down to 250 g cm^{-2}. The intensity at this depth is thirty times that at sea level, and the variation with the depth x is approximately as $\exp(-x/\alpha)$ where α is 220 g cm^{-2}. The differential range spectrum of mesons at sea level has been measured by the same method for ranges between 10 g cm^{-2} and 200 g cm^{-2}. The spectrum is nearly flat in this interval, the value at the lower limit being 0.9 of that at the upper limit. The data which are available in the literature have been examined to obtain the differential range spectrum of mesons whose ranges are greater than 100 g cm^{-2} and less than 3×10^4 g cm^{-2}, and to obtain the variation with altitude of the intensity of fast mesons—mesons with ranges greater than 100 g cm^{-2}.

The experimental results can be explained with the assumption that the number of mesons produced in the depth interval dx at the depth x with ranges in dR at R varies as $G(R)dR\exp(-x/L)dx$. Using 125 g cm^{-2} for L we have arrived at a production spectrum $G(R)$ which is compatible with the experiment data. In the computations, the exact energy-range relation and an empirical atmospheric pressure-altitude relation were used.

The spectrum obtained can be represented approximately by $G(R)=(R+\alpha)^{-2.9}$, where $\alpha=210$ g cm^{-2}. The exact spectrum is of the same form for ranges larger than 100 g cm^2 but falls about 40 percent lower for ranges of 100 g cm^{-2} and less. The observed spectra which result from the derived production spectrum have been computed for several altitudes.

I. INTRODUCTION

LITTLE direct experimental evidence is available concerning the distribution-in-energy of ordinary mesons (mass = 200 electron masses) as they are produced in the atmosphere. It is possible, however, to infer the production spectrum from measurements of the distribution-in-energy of mesons at various locations in the atmosphere, using the known disintegration-probability and energy-loss relations. Various workers have used the measured sea level spectrum of mesons,[1–4] the altitude dependence of the hard component,[5–9] the latitude effect of the hard component,[5–7,10] or the angular dependence and the East–West effect[3,10] to arrive at a production spectrum. Still others[6,11] have obtained production spectra from a knowledge of the spectrum of the primary particles coupled with theoretical reasoning on the nature of the interaction of nucleons. In order to simplify the computations, all of these authors have taken one or more of the following assumptions: (1) That production occurs at one altitude in the atmosphere;[1,3,5,6,9,10] (2) that the energy loss of mesons is independent of their energy[1–3,5,6,8–10] or (3) that the distribution-in-energy at the place of production depends on a negative power of the energy.[1–5,8–10] These approximations are, in general, satisfactory for computations related to the intensity of high energy mesons at sea level, but cannot be expected to give quantitative results concerning measurements on high energy mesons in the upper atmosphere or on low energy mesons ($E<3\mu c^2$) at any altitude.

Although mesons produced with low energy do contribute to the intensity observed at sea level, the contribution is small, and any accurate information about the production spectrum at low energies must be inferred from the slow meson intensity at higher altitudes. In the present work we have attempted to obtain the distribution-in-energy of mesons as they are produced—particularly for low energies—using experimental information on meson intensities. To do this, it was necessary to augment the experimental data available on low energy mesons, and to perform the computations in a manner applicable to such mesons.

In an earlier paper[12] we have reported the results of some measurements of the relative intensity of slow mesons at altitudes up to 10,700 meters. The accuracy of the measurements was impaired at the highest altitudes by the large numbers of spurious events observed. In Part II of the present paper we report the results of some improved high altitude measurements and also of further measurements at sea level made to establish the absolute value of the slow meson intensity.

In reference 12 we reported the results of some preliminary computations which indicated that the slow increase of the low energy meson intensity with altitude implied less production of low energy mesons than would be inferred by an extrapolation to low energies of the production spectrum at high energies. In Part III of

* Most of the material presented here was taken from a thesis submitted in 1948 to the Physics Department, M.I.T., and has appeared also in Technical Report No. 28 (1949) of the Laboratory for Nuclear Science and Engineering. The work was assisted by the Joint Program of the ONR and the AEC.

[1] H. Euler and W. Heisenberg, Ergeb. d. exact. Naturwiss. **17**, 1 (1938).
[2] L. Janossy and J. G. Wilson, Nature **158**, 450 (1946).
[3] E. M. Bruins, Proc. Akad. Wetensch, Amsterdam **42**, 740 (1939).
[4] M. E. Rose, J. Frank. Inst. **236**, 9 (1943).
[5] W. F. G. Swann, J. Frank. Inst. **236**, 111 (1943).
[6] Hamilton, Heitler, and Peng, Phys. Rev. **64**, 78 (1943).
[7] G. Chew, Phys. Rev. **73**, 1128 (1948).
[8] I. Bloch, Phys. Rev. **69**, 575 (1946).
[9] M. Schein and J. Steinberger, Phys. Rev. **72**, 734 (1947).
[10] L. Janossy and P. Nicolson, Proc. Roy. Soc. **192A**, 98 (1947).
[11] Lewis, Oppenheimer, and Wouthuysen, Phys. Rev. **73**, 127 (1948).
[12] Rossi, Sands, and Sard, Phys. Rev. **72**, 120 (1947).

this paper we describe an attempt to synthesize a suitable production spectrum, taking into account the production at all altitudes, the more exact energy-loss relations, and the deviation of the atmosphere from an ideal exponential one. Only those mesons are considered whose trajectories are near the vertical, and lateral scattering effects are neglected.

II. EXPERIMENTS AND EXPERIMENTAL RESULTS

The Altitude Dependence of the Slow Meson Intensity

The experimental results obtained in the previous work[12] suffered the defect that at the highest altitude the counting rate due to mesons was less than that due to chance coincidences. A second set of measurements was made, therefore, with a modified experimental arrangement which is shown in Fig. 1, and which we shall call Arrangement II. The counter tube trays A, B, C, and D correspond to those of the previous set-up and were connected to an identical circuit. Thus, mesons were detected which traversed trays A and B, stopped in the 2.5-cm thick brass absorber S, and gave rise to a disintegration product which traversed both trays C and D in the time interval from 0.9 μsec. to 8.1 μsec. after the arrival of the meson.

With the new arrangement, the delayed coincidence rate due to mesons stopped in S was about the same as before, but the rate of spurious delayed coincidences was less for the following reasons: (a) The rate of twofold coincidences (A, B) was lower because a smaller area and solid angle were subtended by the two trays, and because the layer of lead between trays A and B absorbed much of the very soft electronic component present at high altitudes; (b) the fraction of twofold coincidences (A, B) *not accompanied by the discharge of a tube in tray* C was less, because of the increased extent of tray C; and (c) the rate of twofold coincidences (C, D) was no greater, despite the increased size of the trays, because these trays were shielded by lead at the sides. With Arrangement II, most of the spurious delayed coincidences were due to rays (other than mesons) which traversed trays A and B and stopped in the absorber S.

In order to determine whether the small increase with altitude observed in the first measurements was characteristic only of mesons at the end of their range, or whether it would also hold for mesons of somewhat greater energy, measurements were made with a third arrangement, "Arrangement III," which consisted of Arrangement II with the addition of a 7.5-cm thick layer of lead above in the position indicated by T in Fig. 1.

Seven high altitude flights were made in the summer of 1947 with Arrangements II and III. For these flights the apparatus was mounted in the rear, pressurized cabin of a B-29 aircraft. All flights were made at the latitude of Cambridge. During each flight data were taken at each of two or more altitudes, and at each altitude, with and without the lead in position above the apparatus. The combined data from all flights and from the ground runs are given in Table I for Arrangement II. The data obtained with Arrangement III are given in Table II. The spurious, delayed coincidence rates for all altitudes were computed from the measured twofold and threefold coincidence rates by means of the formula given in reference 12.

The corrected delayed coincidence rates given in Tables I and II depend on the directional intensity of the slow mesons over a rather large angle. Since the angular dependence of the intensity is not known we shall assume that it does not change greatly over the altitudes where the measurements were taken, and that the corrected delayed coincidence rates are, therefore, proportional to the vertical intensity of mesons which could stop in the absorber S. The ratios of the rates at the higher elevations to those at sea level are given in Table III for each arrangement. Included also in Table III are the results from reference 12 under the heading "Arrangement I."

Each of the three experimental arrangements used was sensitive to mesons of different ranges. Table IV gives for each arrangement the mean minimum and maximum ranges in air for mesons which could enter from the vertical and stop in the absorber S. All of the mesons detected are in the "soft component."

It will be seen from Table II that the relative intensities obtained with the three arrangements agree within the errors except for the value obtained with Arrangement II at the lowest atmospheric pressure. Because of

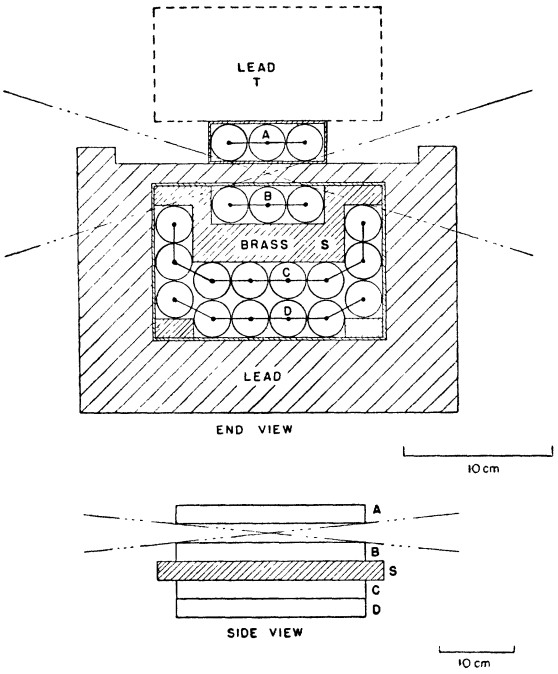

FIG. 1. Experimental Arrangement II.

TABLE I. Experimental results with Arrangement II.

Pressure (g cm^{-2})	1030	610	390	310	250
Approx. alt. (meters)	0	4260	7620	9150	10,700
Twofold coincidences (A, B) (min.$^{-1}$)	107	349	1100	1680	2540
Twofold coincidences (C, D) (min.$^{-1}$)	278	853	2730	4420	5960
Threefold coincidences (A, B, $C+D$) (min.$^{-1}$)	89	260	745	1100	1510
Fourfold coincidences (A, B, C, D) (min.$^{-1}$)	65	188	513	772	1018
Delayed coincidence rate (hr.$^{-1}$)					
0.9–2.7 μsec.	0.61	5.6	10	20	29
2.7–4.5 μsec.	0.33	1.1	6.3	5.2	19
4.5–6.3 μsec.	0.15	1.1	4.2	8.1	13
6.3–8.1 μsec.	0.092	0.4	2.1	6.7	4
Spurious delay rate, each channel (hr.$^{-1}$)	0.009	0.14	1.74	4.6	11
True delay rate, 0.9–8.1 μsec. (hr.$^{-1}$)	1.14±0.03	7.5±1.9	15.3±1.8	22±4.4	20±9
Duration of observations (hr.)	546	2.7	6.7	2.1	0.70

the small number of counts obtained in this measurement the disparity must be allowed as a statistical fluctuation. Thus, we can conclude that within the accuracy of the data the differential intensity of mesons at atmospheric depths down to 250 g cm^{-2} is independent of the range for ranges between 5 and 80 g cm^{-2}, and that the best value for the intensity relative to that at sea level of mesons in the soft component is given by the average of the several determinations at each altitude. Such an average, weighted according to the errors, is given in the last column of Table III. The data of Table III were used in constructing Fig. 7 of Rossi's survey article.[13]

The Intensity of Slow Mesons at Sea Level

The high altitude experiments described above give information about only the relative intensity of slow mesons at the various altitudes. In order to establish an absolute value for the intensity, measurements were made at sea level with experimental Arrangement IV, which is shown in Fig. 2. The counter trays A and B were connected to one of the coincidence circuits, used in the previous experiments. All of the remaining counters were connected in parallel and to *both* of the input terminals of the second coincidence circuit.† The two coincidence circuits were connected to a delay discriminator as before. The delay discriminator was of the same construction as the one used in the previous measurements, but due to a slight variation in the circuit parameters the first channel began at 1.0 μsec. Thus mesons which entered the absorber S via trays A and B were detected if their disintegration product traversed any one of the counters C during the selected time interval. The heavy broken lines in the figure show the locations of a 15-cm thick and a 30-cm thick lead moderator which could be placed in the entrant meson beam. The absorber S in this arrangement was a block of carbon whose density was 1.5 g cm^{-3}.

The condition that the disintegration product produce a coincidence was relaxed, as the equipment was operated only at sea level where the spurious, delayed coincidence rate due to pairs of unrelated rays

TABLE II. Experimental results with Arrangement III.

Pressure (g cm^{-3})	1030	610	390	310	250
Approx. alt. (meters)	0	4260	7620	9150	10,700
Twofold coincidences (A, B) (min.$^{-1}$)	94	251	643	943	1380
Twofold coincidences (C, D) (min.$^{-1}$)	247	662	1800	2700	4000
Threefold coincidences (A, B, $C+D$) (min.$^{-1}$)	85	210	503	709	1000
Fourfold coincidences (A, B, C, D) (min.$^{-1}$)	60	151	359	508	710
Delayed coincidence rate (hr.$^{-1}$)					
0.9–2.7 μsec.	0.58	5.0	7.8	16	23
2.7–4.5 μsec.	0.26	0.4	4.0	5.2	14
4.5–6.3 μsec.	0.15	0	1.8	4.0	7.5
6.3–8.1 μsec.	0.12	0	1.1	2.8	2.5
Spurious delay rate each channel (hr.$^{-1}$)	0.004	0.05	0.45	1.14	2.7
True delay rate, 0.9–8.1 μsec. (hr.$^{-1}$)	1.1±0.07	5.2±1.6	13.0±1.6	23.1±3.3	35±7
Duration of observations (hr.)	216	2.4	5.5	2.5	0.80

[13] B. Rossi, Rev. Mod. Phys. **20**, 537 (1948).

† Actually a preamplifier was interposed between the tubes and the coincidence circuit to compensate for the reduction in signal amplitude which results from connecting many tubes in parallel.

TABLE III. Slow meson intensity relative to that at sea level.

Atmospheric pressure (g cm^{-2})	Relative intensity Arr. I	Arr. II	Arr. III	Average
250	37±6	18±7	32±7	30.5±3.9
310	——	19±4	21±3	20.5±2.6
390	16.1±2.0	13.4±1.9	11.8±1.6	13.5±1.1
610	5.3±0.6	6.6±1.8	4.7±1.5	5.3±0.6
1030	1.00	1.00	1.00	1.00

was negligible. Since all penetrating rays which traversed both trays A and B had to traverse also two counters of tray C, the rate of spurious delayed coincidences due to delays in the discharge of the G-M tubes can be shown to be negligible by the same considerations as before.[12] The experimental results show that the spurious delays are indeed negligible.

Arrangement IV was set up in Cambridge under a wooden roof whose average thickness was about 2 cm, and operated from October 6, 1947 to January 16, 1948. Data were taken with no lead, and with lead moderators 15 cm and 30 cm thick. With each lead thickness data were taken also with the carbon absorber S removed. The following data were taken for each measuring period: (a) The number of twofold coincidences (A, B); (b) the number of threefold coincidences (A, B, C); (c) the number of delayed coincidences (A, B, C_{del}) in each channel; and (d) the counting rate of tray C, which rate was recorded continuously by means of a counting-rate meter. The difference between (a) and (b) gives the number of anticoincidences $(A, B, -C)$, that is, the number of particles which traverse A and B but either stop in S or otherwise fail to trigger a tube in tray C. It will be noted that, while the anticoincidence rate is obtained as a difference, its accuracy does not suffer, because the difference is of two quantities obtained concurrently.

The spurious delayed-coincidence rate due to random pairs of events can be shown to be given for this arrangement by

$$\{A, B, -C\}\cdot\{C\}\cdot\tau, \qquad (1)$$

where $\{A, B, -C\}$ is the counting rate for anticoincidences, $\{C\}$ is the counting rate of tray C, and τ is the width of the interval in which delays are detected.

The data obtained with Arrangement IV are given in Table V. Those obtained with the absorber S removed are given in Table VI.

With no lead moderator the mesons which can be detected must penetrate three G-M tube walls and must stop in the carbon absorber or the walls of G-M tubes immediately adjoining it. With the lead in place the entering mesons must penetrate the additional lead thickness but must stop in the same thickness as before. The mean thickness in the vertical direction of material in which mesons can stop and be detected is equivalent (for mesons) to 16.5 g cm^{-2} of air. The mean range of mesons detected with no moderator is 10 g cm^{-2} of air; with 15 cm of lead it is 100 g cm^{-2}; and with 30 cm of lead it is 200 g cm^{-2}.

TABLE IV. Ranges of mesons which stopped in the absorbers. The ranges are given in g cm^{-2} of air.

Arrangement	Min. range	Max. range
I	5	21
II	13	33
III	63	83

The data indicate that the number of spurious delayed coincidences is negligible. From line 11 in Table VI we see that with the absorber S removed, a total of 14 delayed coincidences were obtained in 299 hr., giving the rate of 0.05 per hr. With the absorber S in place the average delayed coincidence rate is 0.5 per hr. Now, even with absorber S removed, there still remain the walls of the G-M tubes in which mesons can be stopped and give delayed coincidences. The ratio of the thicknesses of stopping material in the two cases is about 0.15. If we assume that the efficiency for detecting disintegration products from the tube walls and from the absorber S is the same, but take into account the fact that, while all mesons which stop in carbon disintegrate, in brass only one-half disintegrate,[14] we conclude that the number of delayed coincidences, to be expected from mesons with S removed, is $(0.5)(0.15)(0.5)=0.03$ per hr. We can therefore conclude that at most 0.02 delayed coincidences per hr. can be due to spontaneous delays in G-M tubes. This is less than the accuracy of the measurements with absorber S in position, and, since presumably it does not depend on the lead thickness, it does not affect appreciably the ratios of counting rates withd ifferent moderators. The above calculation is quite rough, so that the results have not been used to correct the data.

The corrected delayed coincidence rates given in line 13 of Table V are proportional to the differential

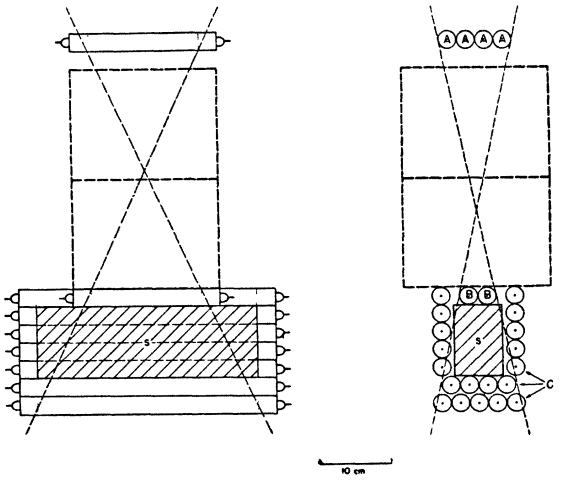

FIG. 2. Experimental Arrangement IV.

[14] G. E. Valley, Phys. Rev. **72**, 772 (1947); **73**, 177 (1948).

intensity of mesons with ranges of 10 g cm^{-2}, 100 g cm^{-2}, and 200 g cm^{-2}. We can obtain from the data the absolute values of the intensities in three more or less independent ways.

(a) We assume that all rays which cause twofold coincidences (A, B) through 15 cm of lead are mesons. Then the difference between the twofold coincidence rates with 15 cm of lead and with 30 cm of lead is a measure of the average, differential intensity of mesons with ranges between 100 and 200 g cm^{-2}. Thus, if we let N_1 and N_2 be the coincidence rates with 15 cm and 30 cm of lead, respectively, R_1 and R_2 the corresponding minimum ranges for mesons detected, and I_0 the vertical intensity of mesons with ranges greater than R_1, the average differential intensity is

$$\bar{\imath}=(I_0/N_1)\cdot(N_1-N_2)/(R_2-R_1). \qquad (2)$$

Unfortunately, fluctuations in meson intensity are a source of error, since the data for different thicknesses of lead were taken at different times. The sets of data were, however, taken over sufficiently long periods that the short period fluctuations should average out. Perhaps the largest remaining effect is due to those fluctuations which are correlated with changes in barometric pressure, and we can make a correction for this. With each day's data the mean barometric pressure for the day was obtained from the U. S. Weather Bureau. From these data the average barometric pressures given in line 14 of Table V were obtained. From the same data and from the daily average counting rates it was found that the average fluctuation with both moderator thicknesses was -13 coincidences per minute for each inch of mercury increase of pressure.‡ If we use this figure to normalize the twofold coincidence data to 30.00 in. of mercury, we find that $(N_1-N_2)=13.3\pm1.0$ (hr.$^{-1}$). We have further that $N_1=198$ (hr.$^{-1}$), and that $(R_2-R_1)=100$ (g cm^{-2}). So we have

$$\bar{\imath}=I_0\frac{13.3}{198(100)}=6.71\times10^{-4}I_0 \text{ g}^{-1}\text{ cm}^2 \text{ of air},$$

with a statistical error of eight percent. If we use the data of Greisen[15] (extrapolated to sea level) we obtain for I_0 the value 0.49 min.$^{-1}$ cm^{-2} sterad.$^{-1}$ Then

$$\bar{\imath}=(3.3\pm0.3)\times10^{-4} \text{ min.}^{-1}\text{ sterad.}^{-1}\text{ g}^{-1}\text{ (of air)}.$$

From the corrected, delayed coincidence rates and the average intensity just computed, we obtain the differential intensities given in the second column of Table VII.

(b) Delayed coincidences are produced by mesons which stop in S, which disintegrate more than 1.0 μsec. but less than 8.2 μsec. after stopping, and whose disintegration product discharges a G-M tube of tray C. If we let f represent the fraction of mesons which disintegrate in the time interval (1.0–8.2) μsec., and g represent the fraction whose disintegration products discharge tray C, then the delayed coincidence rate n is related to the rate n_0 at which mesons stop in S by the equation $n_0=n/fg$. Evidently

$$f=\exp(-1.0/2.2)-\exp(-8.2/2.2)=0.61.$$

An evaluation of g can be made from the known geometry of the counting arrangement and the range in carbon of the disintegration product. We have computed g under the assumption that the range of the disintegration product is 13 cm (20 g cm^{-2}) of carbon, which range is approximately that of an electron whose energy

TABLE V. Data obtained with Arrangement IV, absorber S in place.

(1) Moderator thickness (cm)	0	15	30
(2) Duration of measurement (hr.)	606	284	529
(3) Twofold coincidences (A, B)	176,898	55,861	97,936
(4) Coincidence rate (hr.$^{-1}$)	291.9	196.9	185.1
(5) Counting rate in tray C, (min.$^{-1}$)	2300	2100	1950
(6) Threefold coincidences (A, B, C)	150,054	55,164	96,652
(7) Coincidence rate (hr.$^{-1}$)	247.5	194.4	182.7
(8) Anticoincidences (A, B, $-C$)	26,844	697	1284
(9) Anticoincidence rate (hr.$^{-1}$)	44.3	2.46±0.09	2.43±0.07
(10) Delayed coincidences			
1.0–2.8 μsec.	175	84	168
2.8–4.6 μsec.	77	39	78
4.6–6.4 μsec.	24	13	30
6.4–8.2 μsec.	16	7	12
(11) Total	292	143	288
(12) Spurious delayed coincidences, 1.0–8.2 μsec.	7	0.2	0.3
(13) Corrected delayed coincidence rate (hr.$^{-1}$), 1.0–8.2 μsec.	0.47±0.03	0.50±0.04	0.54±0.03
(14) Average barometric pressure (in. of mercury)	30.07	30.11	29.99

‡ This value agrees with the results of other workers. See, for instance, Rossi, Hilberry, and Hoag, Phys. Rev. **57**, 461 (1940).

TABLE VI. Data obtained with Arrangement IV, absorber S removed.

(1) Moderator thickness (cm)	0	15	30
(2) Duration of measurement (hr.)	69.6	133.4	95.7
(3) Twofold coincidences (A, B)	19,902	26,700	18,065
(4) Coincidence rate (hr.$^{-1}$)	286	200	189
(5) Counting rate in tray C (min.$^{-1}$)	2300	2100	1950
(6) Threefold coincidences (A, B, C)	18,692	26,512	17,944
(7) Coincidence rate (hr.$^{-1}$)	269	197	188
(8) Anticoincidences (A, B, $-C$)	1210	188	121
(9) Anticoincidence rate (hr.$^{-1}$)	17.4±0.5	1.41±0.10	1.26±0.11
(10) Delayed coincidences			
1.0–2.8 μsec.	0	7	1
2.8–4.6 μsec.	1	2	1
4.6–6.4 μsec.	0	1	1
6.4–8.2 μsec.	0	0	0
(11) Total	1	10	3
(12) Spurious delayed coincidences, 1.0–8.2 μsec.	0.3	0.1	0.1
(13) Delayed coincidence rate (hr.$^{-1}$), 1.0–8.2 μsec.	0.01	0.07	0.03

[15] K. I. Greisen, Phys. Rev. **61**, 212 (1942).

is 5×10^7 ev. We obtained for g the value 0.7.¶ Using these values for f and g we find that $n_0=2.3\ n$.

The differential intensity of the mesons which stop in S is then given by

$$i=(n_0I_0)/(N_1t), \tag{3}$$

where N_1 and I_0 are the same quantities used above and t is the thickness (in the vertical direction) of the absorber S. Using the values for N_1 and I_0 above and for t the value 16 g cm^{-2}, we find that

$$i=0.0215\ n\ (\text{g}^{-1}\ \text{sterad.}^{-1}).$$

The intensities obtained from this relation and the data in line 13 of Table V are shown in the third column of Table VII.

(c) We can get values for the differential intensity of mesons with ranges of 100 g cm^{-2} and 200 g cm^{-2} in still another way by using the prompt coincidence data. Twofold coincidences (A, B) not accompanied by threefold coincidences (A, B, C) can arise from the following events: (i) Mesons which traverse trays A and B, and stop in S, but either disintegrate after 1.0 μsec., or give rise to disintegration products which do not traverse tray C; (ii) mesons which traverse A and B and do not stop in S but fail for some reason to discharge C within 1.0 μsec.; (iii) mesons which stop just above tray B and give rise to a disintegration product which traverses B within 1.0 μsec. but are absorbed in S or, otherwise fail to discharge C.

The counting rate of anticoincidences $(A, B, -C)$ due to effect (ii) and to those products considered in (iii) which are not absorbed in S is just the rate given in line 9 of Table VII. An estimate of the rate due to the disintegration products considered in (iii) which do stop in S can be made as follows: Let the range of the disintegration product be 12 g cm^{-2} of lead. The number of mesons which stop in this thickness is equal to the number which would stop in 6 g cm^{-2} of carbon, or 6/15 of the number which stop in S. Of these mesons only 0.5 disintegrate in lead, and of these only $1-\exp(-1/2.2)=0.3$ disintegrate before 1.0 μsec. Of all the disintegration products about 0.3 will traverse tray B and of these about 0.5 will stop in S. From the results of (b) we know that under the 15-cm moderator about $2.2\times0.50=1.1$ mesons stop in S each hour. Thus the anticoincidence rate due to mesons which stop in the lead and whose disintegration products are absorbed by S is approximately $(1.1)(6/15)(0.5)(0.3)(0.3)=0.02$ (hr.$^{-1}$). Since the quantity is small compared to the observed anticoincidence rate with S removed, the crudeness of the estimate will have a negligible effect on the accuracy of the final result. The total anticoincidence rate due to events of the types (i) and (ii) is

¶ The range used was based on the early work of M. Conversi and O. Piccioni, Phys. Rev. **70**, 874 (1946). More recent results of Leighton, Anderson, and Seriff, Phys. Rev. **75**, 1432 (1949), show that a somewhat smaller average range should be used. An estimate using a single range one-half that used above gives for g a value only 15 percent less.

TABLE VII. Differential intensities obtained in three ways.

Mean range (g cm^{-2} of air)	Differential intensity $\times10^{-4}$ min.$^{-1}$ sterad.$^{-1}$ g^{-1} (of air) Method (a)	Method (b)	Method (c)
10	3.0±0.3	1.7±0.1	——
100	3.2±0.3	1.8±0.1	1.8±0.2
200	3.4±0.3	1.9±0.1	1.9±0.2

then (with the 15-cm moderator)

$$(1.41\pm0.10)-0.02=1.39\pm0.10\ (\text{hr.}^{-1}).$$

The observed anticoincidence rate with S in place is 2.46±0.09 hr.$^{-1}$. That due to mesons stopped by S is evidently

$$(2.46\pm0.09)-(1.39\pm0.10)=1.07\pm0.13\ (\text{hr.}^{-1}).$$

This quantity can now be substituted for n_0 in Eq. (3) to obtain the differential intensity. The differential intensities obtained in this way for both moderator thicknesses are given in the last column of Table VII.

The excellent agreement between the results obtained by Methods (b) and (c) is undoubtedly fortuitous. The principle source of error in the determination made by Method (b) is the estimate of the geometric efficiency into which the uncertain range of the disintegration product enters. Also the errors in the values determined by Method (c) are conceivably somewhat larger than the statistical ones since the results depend on the difference between two anticoincidence rates taken at different times. These rates are very sensitive to small changes in the properties of the apparatus, especially to the detection efficiency of tray C. Some confidence in the results, however, may be derived from the fact that Koenig[16] in a similar measurement obtained the value $(2.2\pm0.1)\times10^{-4}$ for the differential intensity of mesons with ranges near 100 g cm^{-2} of air, and that our results agree for both moderator thicknesses. Within the uncertain errors we can conclude from the results of (b) and (c) that all rays which stop under 15 cm and 30 cm of lead are mesons which disintegrate in carbon.

A disturbing feature of the results is the disagreement between the result obtained by the absorption method in (a) and the results obtained by other methods. This discrepancy seems to be larger than can be accounted for by any of the errors in the measurements. It is possible, though it would seem unlikely, that lateral scattering effects are responsible. Mesons of such energy that they should stop in the carbon may be scattered into tray C and produce prompt, threefold coincidences and thus escape detection. The effect is in the proper direction, but it would not account for Koenig's result since the geometry he used was not affected by this kind of scattering. It would seem that the explanation lies elsewhere, and further experiments are necessary to clear up the matter.** At the present time it is probably

[16] H. P. Koenig, Phys. Rev. **69**, 590 (1946).

** For more information on this point see W. Kraushaar, Phys. Rev. **76**, 1045 (1949).

best to assume that the coincidence experiments give the proper absolute value for the differential intensity at ranges greater than 100 g cm^{-2}, and that the delayed coincidence data determine only the relative values for lower ranges. The data of Table VII have been included in Fig. 6 of reference 13.

III. THE PRODUCTION SPECTRUM

The General Problem

We consider the problem of a beam of mesons traveling vertically downward through the atmosphere. We consider the manner in which this beam is enriched by production, is degraded by energy losses, and is depleted by disintegration. For convenience we shall consider a beam of unit cross section (1 cm^2) and by the "number of mesons" in the beam at a level, we shall mean the number which cross that level in a unit of time (1 min.). Depths below the top of the atmosphere and ranges of mesons are measured in terms of the mass per unit area of an equivalent thickness of air. Our unit of thickness will be 100 g cm^{-2}.

The energy of a meson at the atmospheric depth x can be specified by its range $R(x)$ at that depth. Since $dR/dx=-1$, we may write $R(x)=x_0-x$ where x_0 is then a constant which specifies the energy of a given meson at all depths. The depth x_0 will be called the *end point* of a meson. Let $H(R, x)dRdx$ be the number of mesons added to the beam between the depths x and $x+dx$ with ranges (at x) between R and $R+dR$. Then the number of mesons added in dx with end points between x_0 and x_0+dx_0 is $H(x_0-x, x)dx_0dx$. Also let $w(x, s, x_0)$ be the probability that a meson which has the end point x_0 and which is known to be at x will arrive at the depth s before disintegrating. Then, if $F(s, x_0)dx_0$ represents the number of mesons at the depth s which have end points between x_0 and x_0+dx_0, we have

$$F(s, x_0)=\int_{x=0}^{s} H(x_0-x, x)w(x, s, x_0)dx. \quad (s<x_0) \quad (4)$$

The probability $w(x, s, x_0)$ depends only on the energy loss and mean life of mesons and on the properties of the atmosphere. Its computation is carried out below. Equation (4) then relates F, the observable end-point spectrum, to H, the production function of mesons. In what follows an attempt is made to derive H from the experimental data.

The Survival Probability

If we let $p(x, x_0)$ represent the momentum (in units of μc) at x of a meson whose end point is x_0, and $\rho(x)$ the density of air at x; then the probability that the meson survives from the depth r to the depth s is given by the equation

$$-\ln w(r, s, x_0)=\frac{1}{\tau c}\int_r^s \frac{dx}{p(x, x_0)\rho(x)}, \quad (r<s<x_0), \quad (5)$$

where τ is the mean life of a meson at rest and c is the velocity of light. Consider now the function $w(x, x_0)\equiv w(x, x_0, x_0)$, which is the probability that a meson survives from x to its end point. It follows from Eq. (5) that

$$\ln w(r, s, x_0)=\ln w(r, x_0)-\ln w(s, x_0), \quad (6)$$

and that

$$-\ln w(x, x_0)=\frac{1}{\tau c}\int_x^{x_0} \frac{dx'}{p(x', x_0)\rho(x')}, \quad (7)$$

Thus the problem of evaluating the probability function of three variables is reduced to that of taking differences of values of a function of two variables.

The function $p(x, x_0)$ represents the momentum-range relation of mesons in air. The dependence of the range on the density of the air can be neglected,[17] we can, therefore, write $p(x, x_0)=p(x_0-x)$. Also, it is convenient to write

$$\rho(x)=x/[\tau c\zeta(x)],$$

where $\zeta(x)$ is then a slowly varying function of x. Equation (7) takes the form

$$-\ln w(x, x_0)=\int_0^{x_0} \frac{\zeta(x')dx'}{x'p(x_0-x')}. \quad (8)$$

The integral of Eq. (9) has been evaluated for values of x between 0.1 and 10 ($\times$100 g cm^{-2}) and for values of x_0 between 2 and 35 ($\times$100 g cm^{-2}). For vaiues of $x_0>10$, that is, for end points below sea level, we have set $w(10, x_0)\equiv 1$. This is in no way a compromise with accuracy, as it can be shown that, for mesons in solid materials, the probability that a mesons will disintegrate before being brought to rest is negligible compared with any other effects considered here. In order to achieve as great an accuracy as possible, the rest of the integration was carried out numerically using the best available information for p and for ζ.

The function $p(R)$ was obtained from the energy-range relation tabulated by Smith[18] using 10^8 ev/c^2 for the mass of the meson. The function $\zeta(x)$ was computed from the altitude-pressure tables of the National Advisory Committee for Aeronautics for the "United States standard atmosphere"[19] using also $\tau c=6.6\times 10^4$ cm. The standard atmosphere tables represent closely the yearly average atmospheric conditions in the Northern United States. A graph of the function $p(R)$ which we have used appears in Fig. 22 of reference 13. In Fig. 21 of the same paper there is given a graph of the function $x/\rho(x)=\tau c\zeta(x)$.

For a large momenta, that is, for $(x_0-x)>1$, we can evaluate the integral of Eq. (9) in relatively large steps (whose size depends on x_0).

[17] O. Halpern and H. Hall, Phys. Rev. **73**, 477 (1948).
[18] J. H. Smith, Phys. Rev. **71**, 32 (1947).
[19] W. G. Brombacher, N.A.C.A. Report No. 538 (1942).

Consider the partial integral

$$\int^{s} \zeta(x)dx/xp(x_0-x); \quad (r<s<x_0-1). \tag{9}$$

We choose the interval $(s-r)$ as large as possible under the conditions that within the desired accuracy

$$\zeta(x)=\zeta(r)=\zeta(s)$$

and

$$p(x_0-x)=p(x_0-s)+(s-x)\alpha, \tag{10}$$

where α is a constant. The integral (9) can then be evaluated analytically,[1] and becomes

$$\frac{\zeta(s)}{p(x_0-r)+r\alpha}\ln\left[\frac{s}{r}\cdot\frac{p(x_0-r)}{p(x_0-s)}\right], \tag{11}$$

where α depends on the particular x_0, r, and s according to (10). A somewhat larger interval can be used if we take for ζ a mean value between $\zeta(s)$ and $\zeta(r)$.

For small momenta, that is, for $(x_0-x)<1$, it is convenient to rewrite Eq. (9) as

$$-\ln w(x, x_0)=\int_0^{x_0-x} \zeta(x_0-R)dR/(x_0-R)p(R). \tag{12}$$

For $R<0.01$ we can, to a good approximation, set $p(R)=p(0.01)(R/0.01)^{\frac{1}{2}}$ and $x_0-R=x_0$ and evaluate the integral analytically. For $0.01<R<1$ the integrals (12) have been evaluated by straightforward numerical methods.

The probability integrals for $x<x_0-1$ have been obtained from sums of integrals like (12) and terms computed by means of (11). A table of all the values of $w(x, x_0)$ that have been computed is available.[20] A graph of some of the results is given in Fig. 3. In the graph we have plotted $-\ln w(x,x_0)$ against x_0 for various values of x. The probability that a meson whose end point is x_0 will survive between the depths x_1 and x_2 is thus given (see Eq. (6)) by the vertical distance between the curves for x_1 and x_2 at the abscissa x_0.

The Available Data

As the probability function w is completely determined, it is possible in principle to determine the production function H if given sufficient information about the mesons observed in the atmosphere, i.e., about $F(x, x_0)$. The complete range spectrum of mesons at sea level has been measured. (See Part II and reference 13.) We take the solid curve of Fig. 6 in reference 13 to represent $F(s, x_0)$ for $s=10$ ($\times 100$ g cm^{-2}) and for $x_0=R+10$. From the data of Ehmert[21] and of Wilson[22] one sees that this curve can be extrapolated by a straight line to $R=300$ ($\times 100$ g cm^{-2}). We have also information about the altitude dependence of slow mesons (Part II) which give us $F(x_0-0.1, x_0)$ for values of x_0 from 3 to 10 ($\times 100$ g cm^{-2}). In addition, we have information concerning the total hard component at all altitudes.[23] This gives unfortunately little information about the intensity of hard mesons until we make some assumptions about the contributions due to effects other than mesons.

It is assumed here, therefore, that mesons of all energies are produced mainly in the upper atmosphere by the primary radiation and/or by its products. Measurements on the production of penetrating showers and on ionization bursts probably detect the events in which mesons are produced. From an analysis of the data of Janossy[24] and of Tinlot[25] on penetrating showers and of Bridge[26] and Hulsizer[27] one can conclude[13] that events of this type vary with the depth x in the atmosphere in a manner proportional to $\exp(-x/L)$ where L is about 1.25 ($\times 100$ g cm^{-2}). We assume then that the production of mesons in the atmosphere varies also as $\exp(-x/L)$. Since there is not sufficient evidence to decide otherwise we assume further that the mean production depth L is the same for all energies and is 1.25 ($\times 100$ g cm^{-2}).†† We write

$$H(R, x)=G(R)e^{-x/L}. \tag{13}$$

This assumption not only simplifies our task to that of obtaining the energy-dependent part of the production function, but also allows us to obtain the altitude dependence of the intensity of high energy mesons from the hard component measurements. We follow Rossi and take curve *fm* of Fig. 16 in reference 13 to represent the vertical intensity of fast mesons, i.e., mesons with ranges greater than 1($\times 100$ g cm^{-2} of air).

With the assumption we have made regarding the independence of production on depth it is possible in principle to determine the complete production spectrum from the observed, sea level distribution-in-x_0. The method is not practical, however, because it requires a completely impossible accuracy of the experimental data. A more practical method would involve performing the synthesis on the basis of the sea level data and the data on the variation with altitude of the intensity of mesons at the end of their range. Such a method places a large burden on the somewhat uncertain absolute value of the slow meson intensity. In what follows we have therefore attacked the problem in the following way. We have used the sea level spec-

[20] Tech. Report No. 28, see reference *.
[21] A. Ehmert, Zeits. f. Physik **106**, 751 (1937).
[22] V. C. Wilson, Phys. Rev. **53**, 337 (1938).
[23] See Section 3 of reference 13.
[24] L. Janossy, Proc. Roy. Soc. **179A**, 361 (1942).
[25] J. Tinlot, Phys. Rev. **73**, 1476 (1948).
[26] H. Bridge and B. Rossi, Phys. Rev. **71**, 379 (1947).
[27] R. Hulsizer, Phys. Rev. **73**, 1252 (1948).
†† Our assumption implies essentially (a) that the cross section for nuclear interactions of the primary radiation is independent of energy and (b) that the primaries undergo but one meson-producing collision. If there exists a secondary component capable of producing mesons, it is likely that the spectrum of the total meson-producing radiation varies with depth and hence that our separation is not justified.

trum to determine the nature of $G(R)$ for ranges larger than $10(\times 100$ g cm$^{-2})$. The form of $G(R)$ for smaller ranges has then been determined in such a way as to satisfy the data on the altitude dependence of both slow and fast mesons.

The Production Spectrum for Large Energies

In the earlier works mentioned in Part I the authors have shown that if one assumes that all mesons are produced at one altitude—usually taken to be the depth of 1 ($\times 100$ g cm^{-2}), one can explain the observed intensities at sea level for ranges greater than a few $\times 100$ g/cm^{-2} by taking a production spectrum which varies as $R^{-\gamma}$, where γ is about 3. We shall now describe a refinement of this method which not only enables us to obtain the production spectrum for high energies from the sea level data but also points up the limitations in the previous approach.

Consider mesons all of range R produced exponentially in the atmosphere so that the number produced in dx at x is proportional to $\exp(-x/L)dx$. Of those produced in dx the number which arrive at the depth s greater than x but less than R is

$$\phi(x, R, s)dx = e^{-x/L}w(x, s, x+R)dx. \tag{14}$$

Thus, for each meson produced at all depths less than s the number which arrive at s is

$$P(R, s) = \int_0^s \phi(x, R, s)dx. \tag{15}$$

Those mesons which do arrive at s are produced on the average at the depth

$$\bar{x}(R, s) = \int_0^s x\phi(x, R, s)dx \Big/ P(R, s). \tag{16}$$

We are interested in the case where $s=10$ (sea level). In this case it turns out that if $R=10$ the main part of the integrals come from values of x near $\bar{x}$. We can then say approximately that, insofar as the effect at sea level, is concerned, all mesons of range R are produced at the depth $\bar{x}(R, 10)$ and have the probability $P(R, 10)$ of surviving to sea level.

Mesons produced at x with the range R have the end point $x_0=R+x$, or on the average the end point $x_0=R-\bar{x}$. Since this x_0 depends only on R, we can argue as follows: Mesons observed at $s=10$ with end points in dx_0 at x_0 were produced with ranges in $dR=dx_0$ with R given by $R+\bar{x}(R)=x_0$, and were produced at the depth $\bar{x}(R)$ in the number $1/p$ of that observed. By application of this argument we can construct the production spectrum $G(R)$ for $R>10$ from the observed sea level spectrum $F(10, x_0)$ from the relation

$$G(R) = \frac{F(10, R+\bar{x})}{P(R, 10)}. \tag{17}$$

The integrals of Eqs. (15) and (16) have been computed numerically for $s=10$, $L=1.0$,‡‡ and for values of R between 10 and 35 (all$\times 100$ g cm^{-2}). The functions $\bar{x}/L$ and P have been plotted against $x_0=R+\bar{x}$ in the graph of Fig. 4. It is evident that the assumption that all production takes place at $x=L$ is not satisfactory for mesons observed at sea level with end points less than about 12, i.e., with ranges less than two. It is interesting, however, that for all values plotted P is within five percent of $w(1, x_0)$.

The distribution-in-x_0 of mesons observed at sea level has been plotted as curve $i(x_0)$ in Fig. 5. This curve was obtained from the curve of Fig. 6, reference 13, by setting $x_0=R+10$. The curve $G(R)$ was obtained from the curve $i(x_0)$ by application of relation (17). The relation is indicated for a few points by lines joining the two curves. The curve for $G(R)$ obtained in this way is a straight line between $R=10$ and $R=35$. If this line is extended toward larger R's, as indicated by the broken line portion of the curve, it becomes coincident with the curve of $i(x_0)$ at about $R=100$. The data for $i(x_0)$ for x_0's up to 300 (not plotted) also lie on the extrapolated curve of $G(R)$. Since from the curves of Fig. 4, $\bar{x}$ and P both approach one for large R, this is precisely the behavior we would expect if the production spectrum obeyed by a power law. We conclude, therefore, that for ranges between 10 and 300 the distribution-in-range of mesons as they are produced is of the form

$$G(R) = A(R/R_0)^{\gamma}, \tag{18}$$

where $R_0=100$ g cm^{-2}. From the curve of $G(R)$ we find that $\gamma=2.91$, and that if $R_0=100$ g cm^{-2}, $A=207$ min.$^{-1}$ sterad.$^{-1}$ cm^{-2} (100 g cm^{-2})$^{-2}$.

It can be shown that if we had chosen the mean production depth L to be 1.25 ($\times 100$ g cm^{-2}), the above analysis would give a value for γ not significantly different but that A becomes 154 min.$^{-1}$ sterad.$^{-1}$ cm^{-2} (100 g cm^{-2})$^{-2}$.

The curve of $i(x_0)$ suddenly becomes much more steep for values of x_0 greater than 300. From our considerations this would indicate that for high energies the production spectrum no longer obeys the simple law above. Whether this is the case or whether some other phenomena comes into play is not clear. (See, for instance, the discussion of Greisen.[28])

The method of this section is not suitable for determining the production spectrum for ranges less than 10. The difficulty lies in the fact that the function $\phi(x, R, s)$ deviates radically from the general form of an exponential when R and s are less than 10. Thus the integrals (15) and (16) do not receive their main contribution from values of x remote from s and the succeeding arguments are invalidated.

‡‡ At the time these computations were done, $L=1.0$ was the best available value for the mean depth of production. The conclusions of this section would not have been greatly different if the new accepted value, 1.25, had been used.

[28] K. Greisen, Phys. Rev. 73, 521 (1948).

The Production Spectrum for Small R

Referring to Eqs. (4) and (13), it is evident that if we know the production spectrum $G(R)$ we can compute the observed distribution-in-x_0 at any depth s from the equation

$$F(s, x_0)=\int_0^s G(x_0-x)e^{-x/L}w(x, s, x_0)dx. \quad (19)$$

We shall take the measurements of the intensity of slow mesons to give the values of $F(s, s-0.1)\equiv f(s)$. The intensity $I(s)$ of mesons in the hard component at the depth s is related to $G(R)$ by the equation

$$I(s)=\int_{x_0=s+1}^{\infty}\int_{x=0}^{s} G(x_0-x)e^{-x/L}w(x, s, x_0)dxdx_0. \quad (20)$$

The task of evaluating $G(R)$ from $f(s)$ and $I(s)$ in a direct manner by means of Eqs. (19) and (20) is a formidable one. We have, therefore, instead, attempted to select a function $G(R)$ which takes on the form given by (18) for $R>10$ and when entered in Eqs. (19) and (20) yield results in agreement with the data. The process of arriving at a suitable G is made easier by the fact that Eqs. (19) and (20) are linear. Thus, if G_1 yields f_1 and I_1 and G_2 yields f_2 and i_2, then (G_1+G_2) yields (f_1+f_2) and (I_1+I_2). Once the numerical integrations of Eqs. (19) and (20) have been performed for several trial spectra G, these spectra can be used as components of a more complex spectrum with the weights of the various components adjusted so as to give the best fit.

To limit the number of integrations to a finite one, they were carried out only for $s=3$, $s=6$, and $s=10$, where it was felt the experimental data were most reliable. Also this removed the danger of overdetermination of the function G. Of course, G is now underdetermined but requirements of smoothness and reasonableness can carry a share of the burden. The six experimental points which we try to fit by the choice of the production spectrum are given in the first line of Table VIII.

It is evident, from the start, that the production spectrum cannot be given by (18) for all R since then the number and hence the energy of the mesons formed in any finite layer of the atmosphere would be infinite. The first trial functions used were

$$G(R)=10^2\times\begin{cases}R_c^{-2.91}; & R\leq R_c\\ R^{-2.91}; & R\geq R_c,\end{cases}$$

(where all R's are measured in units of 100 g cm^{-2}). Four values were taken for R_c: 1, 2, 4, and 8. These spectra will be referred to be the designations I, II, III, and IV, respectively. The resulting values for $I(s)$ and

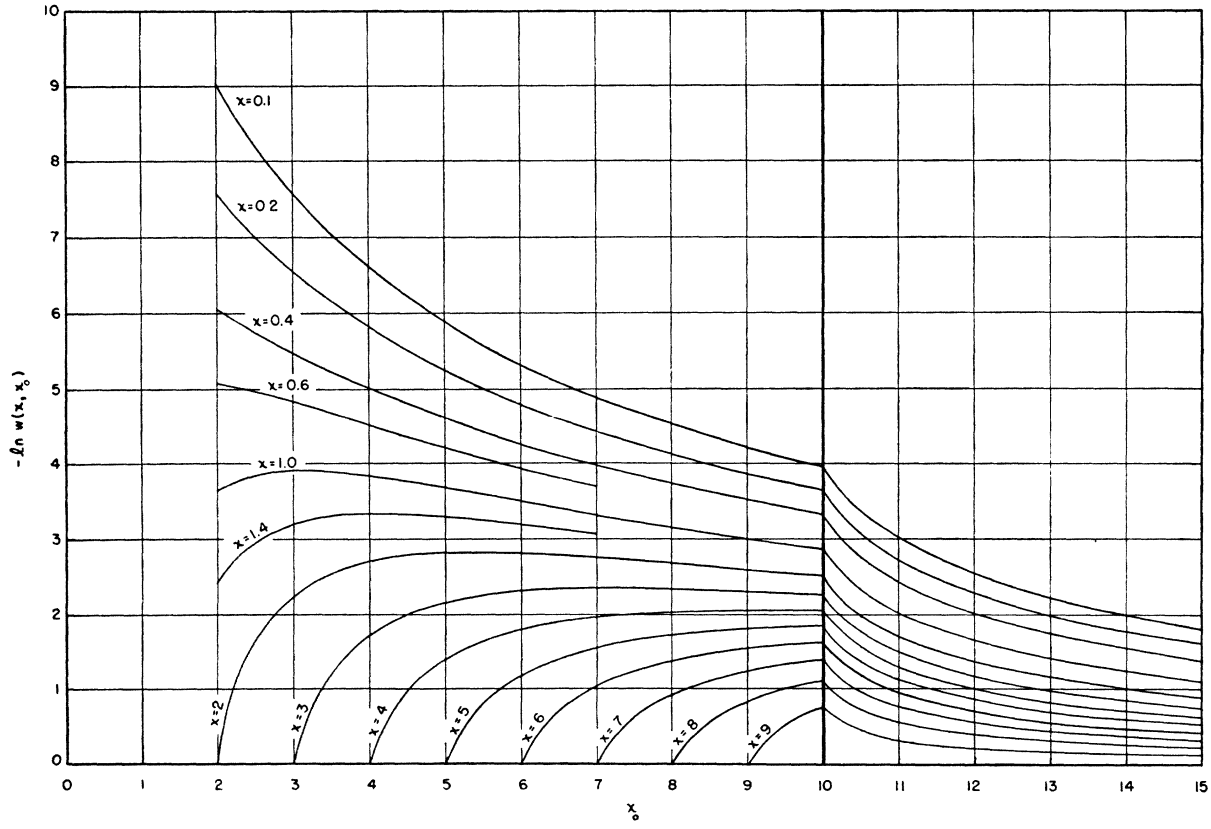

FIG. 3. The survival probabilities. The function $w(x, x_0)$ is the probability that a meson will survive from x to the end of its range at x_0. All depths are measured in units of 100 g cm^{-2}.

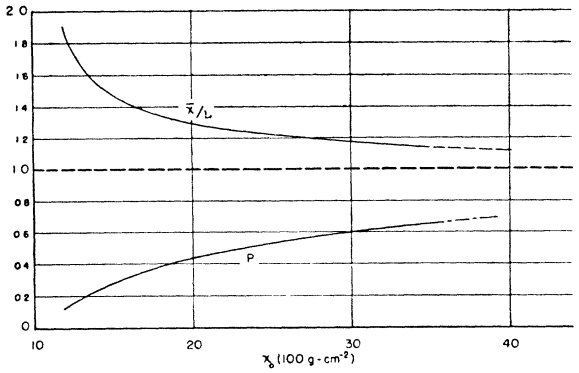

FIG. 4. Mean survival probability and mean depth of production for mesons observed at sea level.

$f(s)$ are given in Table VIII. None of these spectra can be considered as satisfactory, but certainly the general character of the desired spectrum is approached by *III*. It can be shown also that no linear combination of the four spectra is satisfactory.

In order to be able to effect perturbations on the four spectra above for values of R_c less than eight, four other trial functions were used. These are

$$G(R)=10^2\times\begin{cases}(1/R_c^2)(R_c-R); & R<R_c\\ 0; & R>R_c.\end{cases}$$

They are the spectra *V*, *VI*, *VII*, and *VIII* for R_c 1, 2, 4, and 8, respectively. The resulting values for I and f are given in Table VIII.

Since we are trying to fit only six experimental points we can certainly do so with a linear combination of any

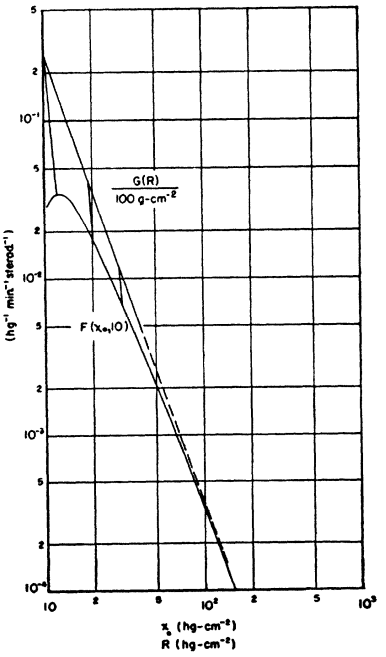

FIG. 5. Distribution-in-x_0 for sea level mesons and the production spectrum for high energies. (Note: hg=100 g.)

TABLE VIII. Observable computed from the various assumed spectra. The number $f(s)$ is the differential intensity of slow mesons at the atmospheric depth s (in 100 g cm^{-2}). $I(s)$ is the intensity of mesons of the hard component at the depth s. The unit for f is min.$^{-1}$ sterad.$^{-1}$ (100 g)$^{-1}$. The unit for I is min.$^{-1}$ sterad.$^{-1}$ cm^{-2}.

	$f(3)$	$f(6)$	$f(10)$	$I(3)$	$I(6)$	$I(10)$
Experimental	0.57	0.142	0.0280	2.40	1.19	0.51
Spectrum *I*	5.10	0.951	0.748	4.11	1.39	0.373
Spectrum *II*	0.91	0.294	0.0395	3.56	1.30	0.371
Spectrum *III*	0.130	0.093	0.0262	2.07	1.00	0.361
Spectrum *IV*	0.0174	0.0153	0.0158	0.86	0.76	0.344
Spectrum *V*	2.20	0.273	0.0134	0	0	0
Spectrum *VI*	2.23	0.287	0.0156	0.49	0.055	0.0038
Spectrum *VII*	1.35	0.345	0.0230	2.75	0.544	0.0231
Spectrum *VIII*	0.1792	0.437	0.077	7.2	2.06	0.158
Spectrum *IX*	0.57	0.151	0.036	2.40	1.34	0.52
Spectrum *X*	0.54	0.124	0.022	1.77	0.81	0.37
Spectrum *XI*	0.56	0.138	0.0278	2.33	1.09	0.50

six of the eight trial spectra we have chosen. We can try to find a suitable combination by inspection. One combination, which was found in this way to give a reasonable fit, yields the spectrum

$$G_{VIII}(R)=0.96G_{III}+0.50G_{IV}+0.20G_V. \qquad (21)$$

The consequences of this spectrum are given with spectrum *VIII* in Table VIII. The computed values agree with the experimental within 30 percent, and the production spectrum is reasonably smooth, being a monatomically decreasing function for all R.

Linear combinations of any six of the trial spectra can be found which give results agreeing exactly with the six experimental values. Five sets of weighting factors for such compound spectra have been obtained (see reference 20 for details). But although all of the spectra so formed fit the six experimental points exactly, and also have the proper form for large R, they could not be considered as satisfactory. First, they were not smooth functions, and second, the resulting function $G(R)$ takes on negative values for some R. The taking on of negative values and the irregularity of the spectra obtained cannot represent the true situation and must be attributed to the properties of the particular trial spectra used. The gross characteristics of all the spectra obtained seem to agree with those of the spectrum given in Eq. (21).

In order to try to abstract the essential characteristics of the compound spectra obtained, we investigated for each (i) the behavior for large R, (ii) the total number of mesons produced. For R larger than eight the spectra all can be expressed

$$G(R)=AR^{-2.91}(R>8).$$

The total number of mesons produced is given by

$$N=L\int_0^\infty G(R)dR.$$

The quantities A for the five compound spectra inves-

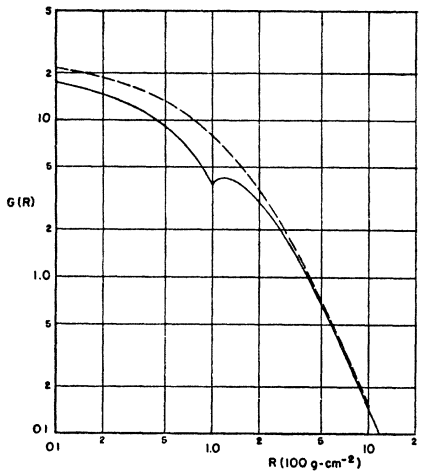

FIG. 6. Distribution-in-range of mesons as they are produced.

tigated all lay near 150, which is in agreement with the value obtained for A in Eq. (18), and the values of N ranged from 23 and 25. We can probably conclude then that the correct spectrum has a value for $A=150$ and for $N=24$.

With this in mind it would seem advisable to try to find a simple, smooth function which is similar to the spectra above and which gives these values for A and N. A function of the form $G(R)=A(R+\alpha)^{-2.91}$ has the general nature of the combined spectra above. The constant A is the same as above and α can be chosen to make the total number of mesons produced be 24. We thus get a new trial spectrum

$$G_X(R)=150(R+2.1)^{-2.91}.$$

The values of $I(s)$ and $b(s)$ resulting from this spectrum are given in line 11 of Table VIII. It is evident that the fit is not very good. Part of the discrepancy can be accounted for by the fact that our requirement that A be the same in this case is too strong. The function G_X differs quite appreciably from $R^{-2.91}$ even for ranges of R as large as 10 or 20. The results also indicate, however, that it is unlikely that a smooth spectrum can be found to fit the data.

As a final attempt we have tried to build a spectrum from a linear combination spectrum X and one of the first eight spectra. The best fit was obtained with the spectrum

$$G_{XI}(R)=1.4G_X-0.04G_I.$$

The consequences of this spectrum are also given in Table VII. The agreement with the experimental data is within three percent for all values but one where it differs by eight percent. The disparity is of the same order as both the experimental errors and the cumulative errors in the numerical computations. We shall therefore consider case XI as our "best" spectrum insofar as the agreement with the altitude data is concerned. It is probably significant that this spectrum gives $N=26$ in close agreement with the "invariant" value obtained for the other combined spectra.

The spectrum $G_{XI}(R)$ has been plotted against R as the solid line in Fig. 6. For comparison the broken-line curve gives $1.4G_X$. The nature of the perturbation $-0.04G_I$ is evident.

It is not clear whether some peculiarity such as the dip at $R=1.0$ in the spectrum of Fig. 6 is necessary in any spectrum compatible with our assumptions. Whether the actual production spectrum is like this, or whether it is due to the inaccuracies of the experimental data, or to one of our basic assumptions cannot be determined by the methods we have used. It is probable, however, that our "best" spectrum represents on the average something close to the true production spectrum averaged over all depths at which production occurs.

Discussion

The properties of the spectrum XI are given in Table IX. The range at production is R in units of 100 g cm^{-2}; the corresponding momentum is $p(R)$ and the total (relativistic) energy $E(R)$, measured in units of μc and μc^2, respectively; $G(R)$ gives the differential range spectrum at production, i.e., $G(R)\exp(-x/L)dxdR$ is the number of mesons produced in dx at x with ranges

TABLE IX. Properties of the production spectrum.

R	$p(R)$	$E(R)$	$G(R)$	$g(R)$	$G_P(p)$	$G_E(E)$
0	0	1	20.42	20.86	0	0
0.1	1.017	1.426	17.34	18.98	4.593	6.450
0.2	1.339	1.671	14.76	17.39	5.246	6.568
0.3	1.601	1.888	12.58	16.02	5.158	6.064
0.4	1.831	2.086	10.73	14.85	4.796	5.419
0.5	2.047	2.278	9.15	13.86	4.300	4.776
0.6	2.256	2.468	7.78	20.46	3.797	4.147
0.7	2.459	2.655	6.60	12.30	3.313	3.571
0.8	2.657	2.839	5.58	11.70	2.845	3.051
0.9	2.852	3.022	4.68	11.19	2.415	2.575
1.0	3.045	3.205	3.89	10.76	2.025	2.142
1.2	3.427	3.570	4.230	9.951	2.220	2.343
1.4	3.806	3.935	4.044	9.119	2.135	2.266
1.6	4.184	4.302	3.701	8.399	1.961	2.036
1.8	4.563	4.671	3.330	7.639	1.761	1.821
2.0	4.941	5.041	2.973	7.008	1.570	1.614
2.2	5.322	5.415	2.650	6.445	1.397	1.425
2.4	5.706	5.793	2.364	5.948	1.241	1.265
2.6	6.089	6.171	2.110	5.495	1.103	1.123
2.8	6.475	6.552	1.890	5.097	0.985	0.998
3.0	6.863	6.935	1.698	4.740	0.8793	0.8878
4	8.835	8.891	1.037	3.409	0.5237	0.5269
5	10.86	10.91	0.6762	2.568	0.3347	0.3361
6	12.92	12.96	0.4650	2.007	0.2260	0.2260
7	15.07	15.10	0.3334	1.613	0.1590	0.1590
8	17.17	17.20	0.2472	1.325	0.1157	0.1157
9	19.38	19.41	0.1884	1.109	0.0871	0.0871
10	21.58	21.60	0.1471	0.9421	0.06708	0.06708
12	26.08	26.10	0.09464	0.7074	0.04221	0.04221
14	30.73	30.75	0.06454	0.5490	0.02814	0.02814
16	35.41	35.42	0.04602	0.4398	0.01970	0.01970
18	40.21	40.22	0.03398	0.3605	0.01430	0.01430
20	44.99	45.00	0.02585	0.3014	0.01073	0.01073
25	57.29	57.30	0.01433	0.2048	0.005731	0.005731
30	69.99	70.00	$0.8774\ 10^{-2}$	0.1484	0.003422	0.003422
35	82.99	83.00	$0.5770\ 10^{-2}$	0.1128	0.002192	0.002192
40	96.00	96.01	$0.4001\ 10^{-2}$	0.0888	0.001488	0.001488

in dR at R (min.$^{-1}$ sterad.$^{-1}$ cm^{-2}) where dx and dR are measured in units of 100 g cm^{-2}. The integral range spectrum is

$$g(R)=\int_R^\infty G(R')dR',$$

and $G_p(p)$ and $G_E(E)$ are the differential momentum and energy spectra, respectively. The differential energy spectrum is also plotted in Fig. 7 as a function of the *kinetic* energy. For comparison the corresponding curve for $1.4\times G_X$ is plotted as the broken line. It will be noted that the differential energy spectrum takes for high energies approximately the form $G_E(E)=kE^{-2.5}$.

For comparison with other data we have plotted by the solid curves in Fig. 8 the differential range spectra of mesons observed at the depths 3, 6, and 10, as a consequence of our final spectrum. We give also, by the broken curve near the $s=10$ curve, the experimental data on mesons at sea level (from Fig. 6, reference 13). That the experimental curve lies below the computed one can be explained in part by the fact that the computations were for the depth 1000 g cm^{-2} and the experimental curve refers to the depth 1030 g cm^{-2}. The broken-line curve near the curve for $s=3$ represents the experimental data obtained by Anderson and co-workers,[29] by momentum measurements at this altitude. For $R>1$ the agreement is within the statistical errors, and for $R<1$ the disagreement probably is due to the fact that no careful separation was made in the experiments of mesons of this range and electrons of the same momentum.

Another check with experiment can be made. Rossi[13] has computed the total energy lost by mesons throughout the atmosphere by the mechanism of collision and disintegration. These computations are based on the complete experimental curves for the fast and slow meson intensities. He finds that the energy lost by mesons is 183 μc^2 min.$^{-1}$ cm^{-2} sterad.$^{-1}$ We can compute the total energy which goes *into* mesons in the atmosphere according to our production spectrum. We find that this energy is 177 μc^2 min.$^{-1}$ cm^{-2} sterad.$^{-1}$ The agreement cannot be completely fortuitous.

From our production spectrum we can obtain a number for the average multiplicity of meson production. From Table IX we see that the vertical "intensity" of all mesons produced in the atmosphere is $L\times g(0.1)=24$ min.$^{-1}$ sterad.$^{-1}$ cm^{-2}. From an examination of the high altitude measurements Rossi[13] concludes that the vertical intensity of the primary radiation is at these latitudes 4.2 min.$^{-1}$ sterad.$^{-1}$ cm^{-2}. We conclude that on the average each primary ray gives rise to $24/4.2=5.7$ mesons.

The results of some of the intermediate steps in our computations show the importance of the contribution to measured intensities of production near the point of observation. Let the integrand of Eq. (19) be represented by $\phi(x, s, x_0)$. Then for a given s and x_0, and hence for mesons of a given range at the point of observation, the magnitude of ϕ at any x is proportional to the contribution to the measured intensity by mesons produced at x. In Fig. 9 we give some of the results from the computation of ϕ. In the figure we have plotted $\phi(x, s, x_0)/F(s, x_0)$ against x for a few values of s and x_0. Then for mesons observed at s with the range x_0-s the ordinate gives the fraction of these mesons that are produced at the depth x (per 100 g cm^{-2} interval). It is evident from these curves that production near the point of observation is predominant for mesons observed at the depth of 300 g cm^{-2} with ranges up to 400 g cm^{-2}; for mesons observed at 600 g cm^{-2} with

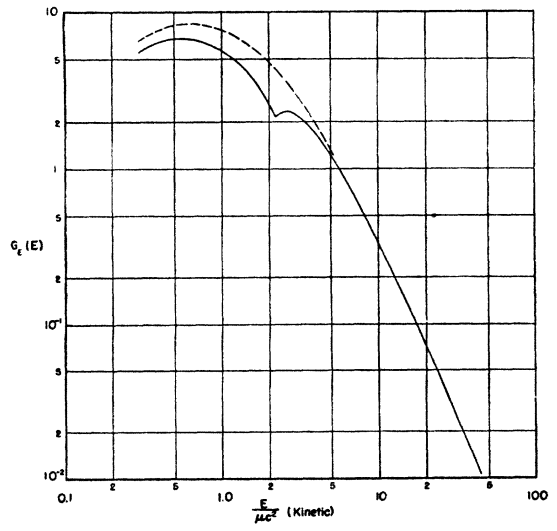

FIG. 7. Distribution-in-energy of mesons as they are produced.

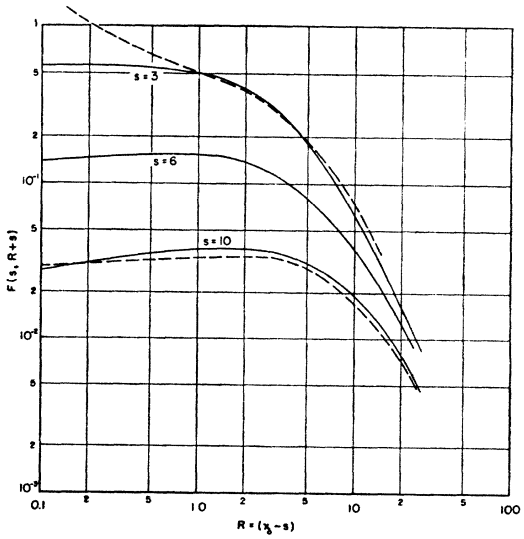

FIG. 8. Predicted differential range spectra of mesons at several altitudes. All thicknesses are in units of 100 g/cm^{-2}.

[29] Anderson, Adams, Lloyd, and Rau, Phys. Rev. 72, 724 (1947).

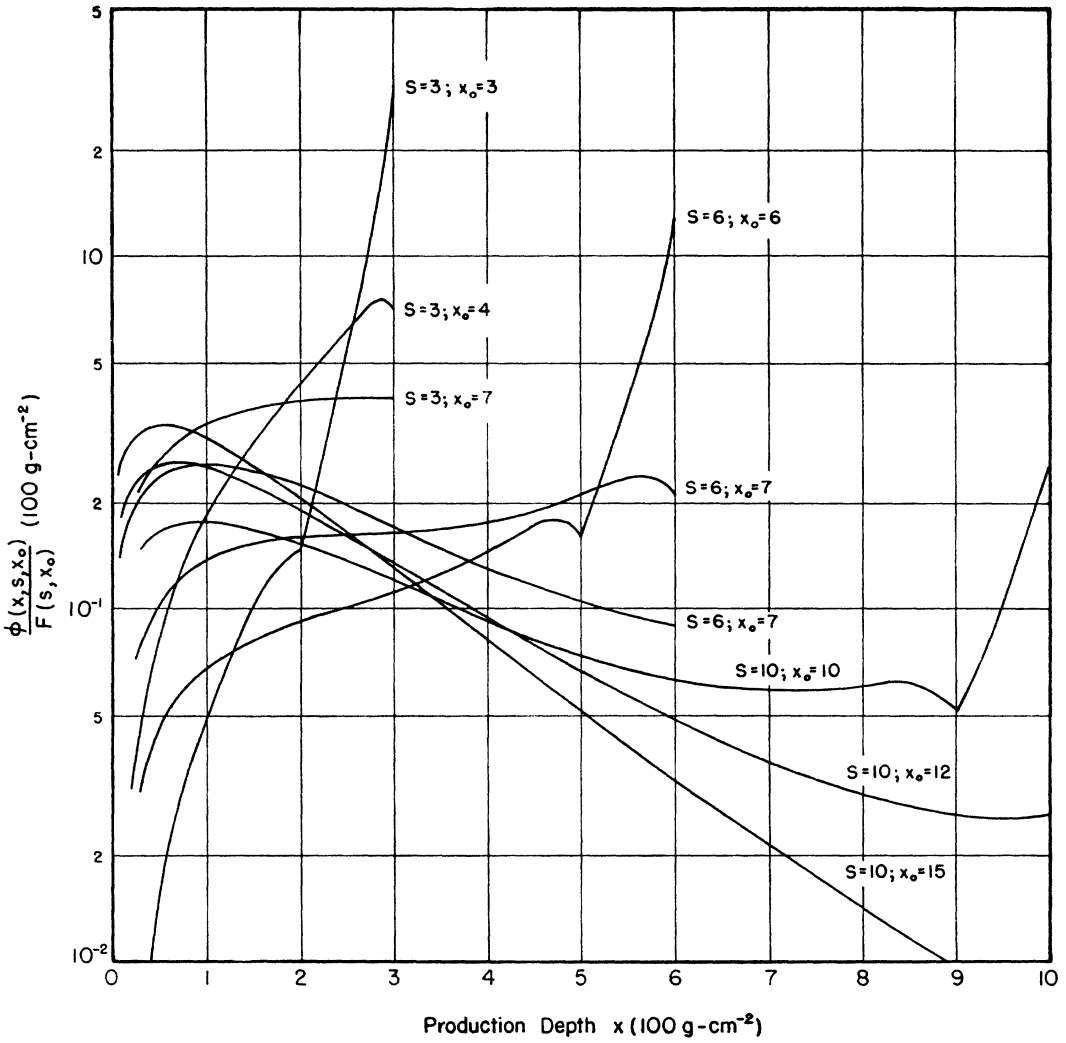

FIG. 9. Production efficiency at various depths for mesons observed at the depth s with the residual range (x_0-s). Note: Near the top of the ordinate scale 10 should read 1.0.

ranges somewhat above 100 g cm^{-2}, and that even at sea level local production cannot be neglected for mesons observed near the end of their range.

CONCLUSIONS

We have shown that it is possible to explain the available data on mesons in the atmosphere under the assumption that the dependences of production on depth and on energy are separable, and that the dependence on depth is as $\exp(-x/1.25)$. A production spectrum has been found which is compatible with these assumptions and with the experimental data. It is not presumed that this spectrum is unique in its details but only that it exhibits the gross properties of any suitable spectrum.

ACKNOWLEDGMENTS

The author is grateful to Professor Bruno Rossi under whose guidance this work was done and to Professor Street of Harvard University whose cooperation contributed to the success of the sea level measurements. P. Bowland, L. Shepard, W. Olney, and W. B. Smith made special contributions to various phases of the work.